Submitted to the 30th International Conference on High-Energy Physics ICHEP2000,
Osaka, Japan, July 2000

Measurement of $D^{*\pm}$ Meson Production and the Charm Contribution to the Proton Structure F_2^c in Deep Inelastic Scattering at HERA

H1 Collaboration

Abstract

The production of $D^{*\pm}(2010)$ mesons in deep inelastic scattering is studied with the H1 detector at HERA using an integrated luminosity of 18.6 pb^{-1}. In the kinematic region $1 < Q^2 < 100$ GeV^2, $0.05 < y < 0.7$ an e^+p cross section for inclusive $D^{*\pm}$ meson production of $8.37 \pm 0.41(stat.)\,^{+1.11}_{-0.82}(syst.)\,^{+0.64}_{-0.39}(theo.)$ nb is measured in the visible range $1.5 < p_T(D^{*\pm}) < 15$ GeV and $|\eta(D^{*\pm})| < 1.5$. Single and double differential inclusive $D^{*\pm}$ meson cross sections are compared to a DGLAP type next-to-leading-order (NLO pQCD) calculation and to calculations using the CCFM evolution. The charm contribution to the proton structure, $F_2^c\,(x, Q^2)$, is determined by extrapolating the visible charm cross section to full phase space.

Abstract: 984
Parallel sessions: 07
Plenary sessions: 03

1 Introduction

Results on D^{*+} meson [1] production in deep inelastic scattering (DIS) and on the charm contribution to the proton structure functionF_2^c at HERA have been published by the H1 and the ZEUS collaborations [1, 2]. Several features of these data show that boson gluon fusion is the dominant source of open charm production in deep inelastic ep scattering: (a) a steep rise of F_2^c with decreasing Bjorken-x, (b) a steep increase of the open charm contribution to DIS from large x accessible at the EMC fixed target experiment [3] towards small x at HERA, and (c) the observed dynamics in inclusive charmed meson production. Therefore, the process $e^+p \to e^+D^{*+}X$ is sensitive to the gluon density in the proton [4] and allows the universality of the gluon density in the proton to be tested by comparing the sensitivities of F_2 and F_2^c.

The early results from the H1 experiment on F_2^c were based on the 1994 data and were therefore statistically limited. The current analysis uses the data of the 1996 and 1997 HERA running periods, yielding a significantly larger integrated luminosity of 18.6 pb^{-1}. Furthermore, the improved instrumentation in the backward region of the experiment enables the kinematic range in four-momentum transfer squared Q^2 of the virtual photon to be extended by one order of magnitude towards smaller values. Hence, more detailed tests of perturbative QCD become possible.

This paper is organized as follows: a short discussion of the different treatments of open charm production in perturbative QCD is followed by a description of the experimental set-up and details of the analysis; the inclusive cross sections of D^{*+} meson production are then presented and are compared to QCD predictions. Finally these inclusive D^{*+} meson cross sections are used to derive the charm contribution to the proton structure function F_2^c.

2 Models of Open Charm Production

The description of open heavy flavor production is based on perturbative QCD (pQCD). In leading order (LO), the photon gluon fusion process ($\gamma g \to Q\overline{Q}$) is the dominant contribution.

2.1 NLO Calculations in the DGLAP Scheme

Several schemes are used to perform NLO calculations. All approaches assume the scale to be hard enough to apply pQCD and to guarantee the validity of the factorization theorem.

Here, the massive approach is adopted which is a fixed order (in α_s) calculation with massive quarks, i.e. $m_Q \neq 0$, assuming three active flavors in the proton. The densities of the three light quarks and the gluon in the proton are obtained by the DGLAP evolution. The heavy quark is assumed to be produced only at the perturbative level [5] via boson gluon fusion. These calculations are considered reliable in the regime $Q^2 \approx m_Q^2$. However, they break down for $Q^2 \gg m_Q^2$ due to large logarithms $\ln(Q^2/m_Q^2)$. Based on the NLO calculations of order α_s^2 in the coefficient functions [6] the Monte Carlo integration program HVQDIS [7] provides the four-momenta of the outgoing partons. Thus the calculation of visible differential inclusive charmed meson production cross sections becomes possible.

[1] The charge conjugate is always implied.

The comparison between the NLO predictions and the data are performed using this Monte Carlo integrator. Charmed quarks are fragmented to D^{*+} mesons according to the Peterson fragmentation function [8], which is controlled by a single parameter ϵ. In addition, to account for the experimentally observed p_t smearing of hadrons with respect to the quark direction, the D^{*+} meson is given a transverse momentum p_t with respect to the charm quark, according to the function $\exp(-\alpha p_t^2)$. The parameter α is chosen such that an average transverse momentum $\langle p_t \rangle \approx 350$ MeV is obtained as observed in e^+e^- data. The fragmentation is performed in the hadronic center mass frame.

2.2 CCFM Evolution

The CCFM evolution equation [9] may be most appropriate to describe the parton evolution at small x. In the parton cascade, gluons are emitted only in an angular ordered region to account for coherence effects. Due to angular ordering, the unintegrated gluon distribution in CCFM depends on the maximum allowed angle in addition to the momentum fraction x and the transverse momentum of the propagator gluon. The cross section is then calculated according to the k_t-factorization theorem by convoluting the unintegrated gluon density with the off- shell boson gluon fusion matrix element with massive quarks for the hard scattering process, well suited for heavy flavor production.

It has previously been shown [10] that F_2 and F_2^c can be reasonably well described within the CCFM framework. Recently. however a solution of the CCFM equation has been obtained [11] which provides a description of F_2 and simultaneously the cross section of forward jet production, a process which is sensitive to non-DGLAP QCD. Using this solution, a full hadron level Monte Carlo generator CASCADE has been developed [12] in which the full generation of charm events, including the initial state gluon radiation according to CCFM and Lund string fragmentation (JETSET) is also possible. The fragmentation of charmed quarks to D^{*+} mesons is performed using the Peterson fragmentation function with ϵ set to 0.078. Here, a refined version of CASCADE with the unintegrated gluon density [13] as extracted from the H1 F_2 data [14] has been used.

3 Detector and Data Sample

The data have been collected with the H1 detector at HERA during the running periods of 1996 and 1997 when HERA operated with 27.5 GeV positrons and 820 GeV protons colliding at a center of mass energy of $\sqrt{s} = 300$ GeV.

While the H1 detector and its trigger capabilities have been described in detail elsewhere [15], the following detector components are significant for this analysis:

The scattered positron is identified and measured in the SpaCal [16], a lead-scintillating fiber spaghetti type calorimeter situated in the backward region of the H1 detector. The SpaCal also provides Time-of-Flight information for trigger purposes. A four-layer backward drift chamber (BDC) [17] is mounted in front in order to improve the angular measurement of the scattered positron.

Charged particles are measured by the cylindrical central jet drift chambers (CJC) [15, 18] mounted concentrically around the beam-line with a homogeneous magnetic field of 1.15 Tesla inside the H1 detector. Particle charge and momenta are measured from track curvature. The CJC also provides trigger information [19] based on the detection of track segments attributed to particles originating at the ep interaction region. One double layer of cylindrical multi-wire proportional chambers (MWPC) [20] for triggering purpose is positioned inside and another one in between the two jet chambers. The events of this analysis were triggered by a coincidence of an electromagnetic cluster in the SpaCal with a charged track signal from the CJC or a crudely reconstructed vertex with the MWPC.

The luminosity is determined from the rate of the Bethe-Heitler reaction $ep \to ep\gamma$. The luminosity system consists of an electron detector and a photon detector located 33 m and 103 m from the interaction point in the electron beam direction, respectively. The data amount to an integrated luminosity of $\mathcal{L}_{int} = 18.6$ pb^{-1}.

4 Kinematics

This analysis is restricted to those deep inelastic scattering (DIS) events which have a scattered positron detected in the backward region of the detector. At fixed center of mass energy, $\sqrt{s}$, the kinematics of the inclusive scattering process $ep \to eX$ can be completely determined by using any two of the independent Lorentz invariant variables: the Bjorken scaling variables x and y, the four-momentum squared $Q^2 = -q^2$ of the virtual boson and the invariant mass squared W^2 of the hadronic final state. In this analysis, these variables are determined from the measurement of the energy E_e' and the polar angle Θ_e of the scattered positron according to the expressions

$$\begin{aligned} Q^2 &= 4E_eE_e'\cos^2\left(\frac{\Theta_e}{2}\right) \qquad & y &= 1 - \frac{E_e'}{E_e}\sin^2\left(\frac{\Theta_e}{2}\right) \\ x &= \frac{Q^2}{ys} \qquad & W^2 &= Q^2\left(\frac{1-x}{x}\right) \end{aligned} \tag{1}$$

where $s = 4E_eE_p$, and E_e and E_p denote the energies of the incoming positron and proton, respectively (positron and proton masses are neglected). Here the scattering angle Θ_e is defined with respect to the proton beam direction.

5 Monte Carlo Simulation

Monte Carlo simulation programs are used in order to correct the data and to estimate the systematic uncertainties associated with the measurement. For the determination of the acceptance of the detector and the D^{*+} selection efficiencies, heavy flavor (charm and bottom) DIS events are generated using the AROMA 2.2 [21] program. This simulates neutral current heavy quark production via the boson gluon fusion process and is implemented in leading order QCD including heavy quark mass effects. The charmed quark mass is chosen to be $m_c = 1.5$ GeV while the factorization and renormalization scales were set to $\mu = \hat{s}$. The GRV94LO [22] parton density functions (PDF's) are used for the proton. The Lund Model [23], as implemented in JETSET 7.4 [24] including the parton shower option, is used for hadronization. The momentum fraction of the charm quark carried by the D^{*+} meson is determined according to the Peterson model [8] using a fragmentation parameter ϵ of 0.078. In order to study the effect of different fragmentation models on the acceptance and efficiencies in the AROMA program, the Peterson fragmentation parameter is varied between $\epsilon = 0.035$ and $\epsilon = 0.1$, and, in addition, the symmetric Lund fragmentation function has been used. Furthermore, the HERWIG [25] event generator is used with the same charm quark mass and the same PDF's for this purpose. In order to investigate the effect of the QCD parameters the charm quark mass has been varied between $m_c = 1.3$ GeV and $m_c = 1.7$ GeV and the renormalization scale is changed to $\mu = Q^2 + 4m_c^2$. The influence of QED effects at the leptonic vertex is determined with help of the RAPGAP [26] program interfaced to HERACLES 4.1 [27]. All Monte Carlo generated events are fed into the GEANT based simulation program [28] of the H1 detector and are subjected to the same reconstruction and analysis chain as used for the data.

6 Event Selection

6.1 Selection of DIS Events

The identification and selection of the scattered positron in the SpaCal is performed with minor changes, as described in Ref. [29].

The positron is identified as the most energetic cluster with $E_e > 8$ GeV. The cluster radius[2] is required to be less than 4 cm, consistent with an electro-magnetic energy deposition, and the cluster center of gravity is required within 1.5 cm of the extension of a charged track segment in the backward drift chamber BDC [17].

The geometrical acceptance cuts for SpaCal and BDC impose a limitation on the positron scattering angle of $\Theta_e < 178°$. This requirement restricts the accessible range of the negative four momentum squared of the photon to 1 GeV^2 $< Q^2 <$ 100 GeV^2 and the inelasticity to $0.05 < y < 0.7$.

Figure 1 shows the energy and polar angle distributions of the scattered positron for events with identified D^{*+} mesons. The data include corrections for QED radiation as described below. The figure also includes the absolute prediction of the AROMA Monte Carlo for all values of Q^2. Good agreement is observed between data and simulation. The contribution due to photoproduction background, i.e. $Q^2 < 1$ GeV^2, amounts to less than 1%.

6.2 Selection of Events with D^{*+} Mesons

D^{*+} mesons are reconstructed using the decay chain

$$D^{*+} \to D^0 \pi^+_{slow} \to (K^- \pi^+) \pi^+_{slow}. \tag{2}$$

The identification of charm production using the D^{*+} tagging technique [30] profits from the tight limitation of phase space in the decay $D^{*+} \to D^0 \pi^+_{slow}$.

The decay products are detected in the central tracker. For each observed track passing some quality cuts and fulfilling minimum transverse momentum requirements particle identification

[2] The cluster radius is defined as $\sum_i \log(E_i) \cdot d_i / \sum_i \log(E_i)$ where the sum runs over all cells in the cluster: E_i is the energy of the cell i and d_i is the distance of the cell i from the cluster center of gravity.

is applied using the measurement of the energy loss $\mathrm{d}E/\mathrm{d}x$ in the central tracker. A resolution of 6% is reached for well measured tracks. For each track, the probability of the pion, kaon and proton hypothesis is calculated from the measurement of the energy loss along the trajectory. Assuming the observed track to be produced by either of these particle species, normalized probabilities are calculated. Only those tracks are considered which may be interpreted as pions or kaons, by passing momentum dependent minimum values for the corresponding normalized probabilities.

In order to reconstruct a D^{*+} meson candidate, unlike-sign charged tracks are first combined to form $K^-\pi^+$ pairs, i.e. one of the tracks should allow the kaon interpretation according to its $\mathrm{d}E/\mathrm{d}x$ measurement while the other must be consistent with the pion hypothesis. Among all possible oppositely charged $K^-\pi^+$ pairs, those with an invariant mass consistent within $\pm$70 MeV of the D^0 are combined with a track of a second pion candidate ("π^+_{slow}") having a charge opposite in sign to that of the kaon.

The distribution of the mass difference $\Delta m = m_{K\pi\pi} - m_{K\pi}$ is shown in Fig. 2 for the $K\pi\pi$ combinations in the acceptance range of pseudorapidity, $\eta(K\pi\pi) = -\ln\tan(\Theta_{K\pi\pi}/2)$, and transverse momentum $p_t(K\pi\pi)$. This range is restricted to $|\eta(K\pi\pi)| < 1.5$, and $p_t(K\pi\pi) > 1.5$ GeV. A distinct enhancement is visible around the nominal $D^{*+} - D^0$ mass difference of 145.4 MeV. This figure also includes a Δm distribution for particle combinations in which the $K\pi$ pairs are formed by like-sign charged tracks. This distribution is exclusively determined by track combinatorics. No enhancement is observed in the Δm distribution in this case. Furthermore the like-sign distribution gives a perfect description of the unlike-sign background. The number of D^* mesons N_{D^*} is extracted from fits to both Δm distributions with a function taken to be the superposition of a Gaussian for the signal and a term $N_B(\Delta m - m_\pi)^\alpha$ for the background. A total of 973 ± 40 D^{*+} mesons is observed.

7 Inclusive Cross Sections

The integrated and differential cross sections for D^{*+} meson production in DIS ep collisions are calculated from the observed number N_{D^*} of D^{*+} candidates, according to

$$\sigma(e^+p \to e^+D^{*+}X) = \frac{N_{D^*}\,(1-r)}{\mathcal{L}_{int}\cdot B\cdot\epsilon\cdot(1+\delta_{rad})}\,. \tag{3}$$

Here, r stands for the contribution of reflections in the D^0 mass window, amounting to 3%, while $\mathcal{L}_{int}$ and B refer to the integrated luminosity and the branching ratio $B = B(D^{*+} \to D^0\pi^+)\cdot B(D^0 \to K^-\pi^+) = 0.0263$ [31]. The efficiency ϵ is estimated with help of the AROMA Monte Carlo program [21]. The radiative corrections δ_{rad}, which amount to $\delta_{rad} = 0.03$ for the integrated visible cross section, are obtained from the program HECTOR [32].

7.1 Integrated Cross Section

The inclusive cross section of D^{*+} meson production in the kinematic region 1 GeV^2 $< Q^2 <$ 100 GeV^2, $0.05 < y < 0.7$ and in the visible D^{*+} range $|\eta(D^{*+})| < 1.5$ and $p_t(D^{*+}) > 1.5$ GeV is found to be

$$\sigma_{vis}(e^+p \to e^+D^{*+}X) = \left(8.37 \pm 0.41(stat.)\,{}^{+1.11}_{-0.82}(syst.)\,{}^{+0.64}_{-0.39}(theo.)\right)\ \mathrm{nb}.$$

The errors refer to those from statistics, experimental systematics and an additional systematic error related to the changes in efficiency obtained using different Monte Carlo generators and varying the model parameters.

The largest contribution to the experimental systematic error is due to the uncertainty in the track reconstruction efficiency. Other important sources of systematic errors include uncertainties in the extraction of the D^{*+} signal, i.e. the determination of the background shape in the Δm distribution and of the D^0 mass resolution, and the uncertainty in the branching fraction of the D^{*+} to $K\pi\pi$ from other experiments. By adding the different contributions in quadrature, a total relative error of $^{+12\%}_{-10\%}$ is obtained for the integrated cross section.

The uncertainties due to model dependences include our incomplete understanding of the fragmentation process, the uncertainty due to the charm quark mass, the sensitivity to the factorization and renormalization scales μ and the change of acceptance due to QED effects on the lepton side. The largest effect on the efficiency is observed by changing the charm quark mass from $m_c = 1.5$ GeV in the reference Monte Carlo dataset to $m_c = 1.3$ GeV. A total relative model dependent error of $^{+8\%}_{-5\%}$ is obtained by adding the different contributions in quadrature.

In the framework of the NLO DGLAP evolution, the visible inclusive D^{*+} meson production cross section has been calculated with the HVQDIS program. The predictions range from 4.98 nb for a charm quark mass $m_c = 1.5$ GeV and Peterson fragmentation parameter $\epsilon = 0.10$ to 6.61 nb for $m_c = 1.3$ GeV and $\epsilon = 0.035$ using the GRV-HO 98 parton densities in the proton [33]. The hadronization fraction $f(c \to D^{*+})$ was set to the world average $0.235 \pm 0.007 \pm 0.007$ [34]. On the other hand calculations based on the CCFM evolution, as implemented in the CASCADE program, yield a significantly higher cross section, 8.53 nb for $m_c = 1.5$ GeV and 9.95 nb for $m_c = 1.3$ GeV, using a fragmentation parameter $\epsilon = 0.078$ and the unintegrated gluon density as extracted from the H1 F_2 data [13].

The NLO DGLAP prediction does not describe well the measured values. In previous publications [1, 4] H1 reported much better agreement between data and predictions from the HVQDIS program. This difference in the interpretation of the measured visible D^{*+} meson cross section is due to the new determination of the charm quark hadronization fraction $f(c \to D^{*+})$ which result in a value 16% smaller than previously measured.

7.2 Differential Cross Sections

In Fig. 3 the inclusive single differential D^{*+} cross sections in the visible region are shown as a function of the kinematic quantities W, x_{Bj} and Q^2 and as a function of the D^{*+} observables $p_t(D^*)$, $\eta(D^*)$ and $z_D(D^*) = P \cdot p_{D^*}/P \cdot q = (E - p_z)_{D^*}/2yE_e$ (P, q and p_{D^*} denote the four-momenta of the incoming proton, the exchanged photon and the observed D^{*+}). The errors account for the statistical error (inner error bars) and the total error (outer error bars) obtained by adding the statistical error and the systematic uncertainties in quadrature. A bin by bin correction due to QED radiation has been applied using the HECTOR program [32] amounting to 3% for the full kinematic range.

Also shown in Fig.3 are the expectations from the NLO QCD calculations of the HVQDIS program using the GRV 98 HO parton density parameterization [33], a charm quark mass varying from $m_c = 1.3$ GeV to $m_c = 1.5$ GeV and a fragmentation parameter varying from $\epsilon = 0.035$ to $\epsilon = 0.10$. The renormalization scale and the factorization scale are set to $\mu_r^2 = \mu_f^2 = Q^2 + 4m_c^2$. The dark shaded band indicates the uncertainties in this calculation for $m_c = 1.3$ GeV and $\epsilon = 0.035$ (upper limit) and $m_c = 1.5$ GeV and $\epsilon = 0.10$ (lower limit). Although the predicted visible cross section is smaller than experimentally observed, the agreement with the data in the shapes of the different single differential cross sections is reasonable. A difference in shape is observed only in the shape of the $\mathrm{d}\sigma/\mathrm{d}\eta$ cross section. In the forward direction, the observed D^{*+} meson production cross section is considerably larger than predicted by the calculation. This excess is also manifest in the larger cross section observed in the data at small z_D.

A possible cause for this effect could be the simplified implementation of fragmentation in the HVQDIS program. This approach does not account for the color force between the charm quark and the proton remnant which should result in a migration of the D^{*+} meson from the original charm quark direction towards larger pseudorapidities. To quantify this 'beam drag effect' [35], a mapping function from $\eta(c)$-$p_t(c)$-space to $\eta(D^{*+})$-$p_t(D^{*+})$ space has been constructed with help of the AROMA Monte Carlo program. This function has then been used to replace the Peterson fragmentation with transverse momentum smearing in HVQDIS. No significant change in the η and z_D distributions have been observed by this procedure compared to the original treatment of fragmentation.

Figure 3 also includes the predictions of the CCFM calculations using the CASCADE program. Here, the charm quark mass is varied from $m_c = 1.3$ GeV (upper limit) to $m_c = 1.5$ GeV (lower lower) while the Peterson fragmentation parameter is fixed to $\epsilon = 0.078$. The expectations from the CASCADE program are found to agree better with data in general and especially in the forward η region, where the HVQDIS program fails to describe the data. It is interesting to note that the CCFM calculation, which starts from completely different principles and aims specifically to describe low x phenomena, is able to describe open heavy flavor production in the HERA regime better than the DGLAP based NLO calculations with the chosen settings.

In order to enable the study of correlations among the observables in D^{*+} meson production Figures 4 and 5 show double differential inclusive D^{*+} cross sections. It is evident that the excess observed in the data with respect to the HVQDIS expectation at large pseudorapidities ($0.5 < \eta < 1.5$) is independent of Q^2 and is concentrated at small $p_t(D^{*+})$ and small z_D. It is especially in this phase space region where the CASCADE program better represents the data. In general this program leads to a better description of the data for small transverse momenta of the D^{*+} mesons ($p_t < 4$ GeV). At larger transverse momenta the predictions of the HVQDIS program agree better with the data.

8 Charm Contribution to the Proton Structure F_2^c

The charm contribution $F_2^c(x, Q^2)$ to the proton structure function is obtained by using the expression for the one photon exchange cross section for charm production

$$\frac{d^2\sigma^c}{dxdQ^2} = \frac{2\pi\alpha^2}{Q^4 x}\left(1 + (1-y)^2\right)\ F_2^c(x, Q^2)\ . \tag{4}$$

The range of y of the measurements is such that contribution from the second structure function F_1 is everywhere negligible.

The visible inclusive D^{*+} cross sections $\sigma_{\mathrm{vis}}^{\mathrm{exp}}(x, Q^2)$ in bins of x and Q^2 are converted to a bin center corrected $F_2^{c\ \mathrm{exp}}(\langle x\rangle, \langle Q^2\rangle)$ by the relation:

$$F_2^{c\ \mathrm{exp}}(\langle x\rangle, \langle Q^2\rangle) = \frac{\sigma_{\mathrm{vis}}^{\mathrm{exp}}(x, Q^2)}{\sigma_{\mathrm{vis}}^{\mathrm{theo}}(x, Q^2)} \cdot F_2^{c\ \mathrm{theo}}(\langle x\rangle, \langle Q^2\rangle)\ , \tag{5}$$

where $\sigma_{\rm vis}^{\rm theo}$ and $F_2^{c\ {\rm theo}}$ are the theoretical predictions from the model under consideration. Following the same line as in previous publications [1, 2, 4] the HVQDIS program and the program of Ref. [5] is used to calculate these quantities in next to leading order.

In Fig. 6, the charm contribution to the proton structure function F_2^c is shown as a function of x for different bins in Q^2 with $m_c = 1.4$ GeV as extracted from the inclusive D^{*+} cross sections. The error bars correspond to the statistical and total experimental errors. Also shown is the expectation using the result from the H1 NLO DGLAP fit to the inclusive F_2 measurement [36]. The band indicates the uncertainty in this extraction introduced by varying the charm quark mass between 1.3 GeV and 1.5 GeV. Other sources of uncertainties in the determination of the gluon density in the proton are not yet taken into account. The direct measurement of F_2^c suggests a steeper rise at small Q^2 than expected from the calculations based on the gluon density in the proton extracted from the inclusive F_2 measurement.

The extraction of F_2^c according to Equation 5 is faced with an intrinsic problem. Since the determination of $F_2^{c\ exp}$ includes the extrapolation from the visible range of D^{*+} meson production to full phase space, the measured value $F_2^{c\ exp}$ depends on the predicted acceptance of the theoretical calculation for a given choice of parameters. Therefore the results on F_2^c are shown also in the framework of the CCFM evolution separately in Fig. 7 as a function of x for different bins in Q^2. As in the previous figure, F_2^c is shown for $m_c = 1.4$ GeV. However, the CASCADE program is used to extract F_2^c from the inclusive D^{*+} cross sections in this case. The figure includes also the prediction according to the CCFM evolution using the unintegrated gluon density [13] as extracted from the inclusive F_2 measurement of H1. The band indicates the uncertainty on this prediction due to the variation of the charm quark mass between 1.3 GeV and 1.5 GeV.

The comparison of Fig. 6 and Fig. 7 reveals a steeper rise in the predicted charm contribution to the proton structure towards small x in the CCFM evolution than obtained by the NLO DGLAP evolution. Using the acceptances as calculated with the CASCADE program the measured values of F_2^c are found to be systematically smaller than those determined with the HVQDIS program. Especially at small x differences up to almost 20% are observed, significantly larger than the statistical uncertainty on the data.

In Fig. 8 the charm contribution to the proton structure function F_2^c is shown as a function of Q^2 for different bins in x in the NLO DGLAP picture. As in Fig. 6 the bands indicate the NLO predictions for m_c varying between 1.3 GeV and 1.5 GeV and using the parton densities in the proton obtained from the H1 NLO fit to the inclusive F_2. The variation of the slope of the Q^2 dependence of F_2^c with x tends to be stronger for the data than expected by this calculation.

9 Conclusions

New results on differential inclusive D^{*+} meson production cross sections in deep inelastic ep scattering from the 1996 and 1997 H1 data have been presented. The measured visible cross section is found to be larger than predicted by the NLO HVQDIS program using the GRV-HO 98 parton densities in the proton and a Peterson fragmentation function with transverse momentum smearing. From the results on the single and double differential cross sections the phase space region in the D^{*+} meson production dynamics responsible for this difference is singled out to the forward pseudorapidity and small p_t region. The predictions of the CCFM based CASCADE program are in better agreement with the data than those from HVQDIS.

By extrapolating the visible D^{*+} meson production cross section to full phase space in $p_t(D^{*+})$ and $\eta(D^{*+})$, the charm contribution to the proton structure F_2^c has been extracted in the framework of NLO DGLAP and of CCFM QCD. Compared to the previous H1 study, the kinematic range has been extended down to $Q^2 = 1.5$ GeV^2. The data exhibit large scaling violations as well as a steep rise of F_2^c towards small x. This rise tends to be steeper than expected from the NLO DGLAP evolution while it agrees well with the CCFM based calculations.

References

[1] C. Adloff *et al.* (H1 Collaboration), Z. Phys. C72(1996)593.

[2] J. Breitweg *et al.* (ZEUS Collaboration), Phys. Lett. B407(1997) 402; Euro. Phys. J. C12 (2000) 1.

[3] J. J. Aubert *et al.* (EMC Collaboration), Nucl. Phys. B213 (1983) 31.

[4] C. Adloff *et al.* (H1 Collaboration), Nucl. Phys. B545 (1999) 21.

[5] E. Laenen *et al.*, Nucl. Phys. B392 (1993) 162, 229; E. Laenen *et al.*, Phys. Lett. B291 (1992) 325; S. Riemersma, J. Smith, and W.L. van Neerven: Phys. Lett. B347 (1995) 143.

[6] B.W. Harris and J. Smith, Nucl. Phys. B452 (1995) 109, Phys. Lett. B353(1995)535.

[7] B.W. Harris and J. Smith, Phys. Rev. D57 (1998) 2806.

[8] C. Peterson *et al.*, Phys. Rev. D27(1983)105.

[9] M. Ciafaloni, Nucl. Phys. B296 (1988) 49; S. Catani, F. Fiorani and G. Marchesini, Phys. Lett. B234 (1990) 339; Nucl. Phys. B336 (1990) 18; G. Marchesini, Nucl. Phys. B445 (1995) 45.

[10] J. Kwieciński, A.D. Martin and P.L. Sutton, Phys. Rev. D53 (1996) 6094; Z. Phys. C71 (1996) 585.

[11] H. Jung, Proc. 7th DIS Workshop, Nucl. Phys. B (Proc. Suppl.) 79 (1999) 429;hep-ph/9905554.

[12] H. Jung, Proc. Workshop on Monte Carlo Generators for HERA Physics, 1999, DESY-PROC-1999-02, p.75; hep-ph/9908497; H. Jung and G. Salam, to be published.

[13] S.P. Baranov, H. Jung and N.P. Zotov, Proc. Workshop on Monte Carlo Generators for HERA Physics, 1999, DESY-PROC-1999-02, p.484.

[14] S. Aid *et al.*, Nucl. Phys. B470 (1996) 3.

[15] I. Abt *et al.* (H1 Collaboration), Nucl. Instr. Meth. A386 (1997) 310 and 348.

[16] R.D. Appuhn *et al.* (H1 SpaCal group), Nucl. Inst. Meth. A386 (1997) 397.

[17] H1 Collaboration, Technical proposal for the upgrade of the backward region of the H1 detector, DESY internal report PRC-93/02.

[18] J. Bürger *et al.*(H1 Collaboration), Nucl. Inst. Meth. A279 (1989) 217.

[19] T. Wollf *et al.*, Nucl. Inst. Meth. A323 (1992) 537.

[20] K. Müller *et al.*, Nucl. Inst. Meth. A312 (1992) 457.

[21] G. Ingelman, J. Rathsman and G.A. Schuler, Comp. Phys. Comm. 101(1997)135.

[22] M. Glück, E. Reya and A. Vogt, Z. Phys. C67(1995)433.

[23] B. Anderson, G. Gustafson, and B. Söderberg, Z. Phys. C20 (1983) 317; M.G. Bowler, Z. Phys. C11 (1981) 169; D.A. Morris, Nucl. Phys. B313 (1989) 634.

[24] T. Sjöstrand, Comp. Phys. Comm. 82 (1994) 74.

[25] G. Marchesini *et al.*, Comp. Phys. Comm. 67 (1992) 465.

[26] H. Jung, Comp. Phys. Comm. 86 (1995) 147.

[27] A. Kwiatkowski, H. Spiesberger and H.J. Möhring, Proc. of the 1991 Workshop on Physics at HERA, DESY, Hamburg, Vol. 3 (1992) 1294; Z. Phys. C 50 (1991) 165.

[28] R. Brun *et al.*, CERN DD/EE/84-1 (1987).

[29] C. Adloff et al. (H1 Collaboration), Nucl. Phys. B497(1997)3..

[30] G. Feldmann *et al.*, Phys. Rev. Lett. 38 (1977) 1313.

[31] C. Caso *et al.* (Particle Data Group),Eur. Phys. J.(1998)1

[32] A. Arbuzov *et al.*, Comp. Phys. Comm. 94 (1996) 128.

[33] M. Glück, E. Reya and A. Vogt, Eur. Phys. J. C5 (1998)461-470.

[34] R. Barate *et al.*(ALEPH Collaboration), CERN-EP-99-094, submitted to Eur. Phys. J. C.

[35] E. Norrbin, hep-ph/9909437; E. Norrbin and T. Sjöstrand, hep-ph/0005110.

[36] C. Adloff *et al.* (H1 Collaboration), Contributed paper to the 30th International Conference on High-Energy Physics ICHEP2000, Osaka, Japan, July 2000 abstract 945

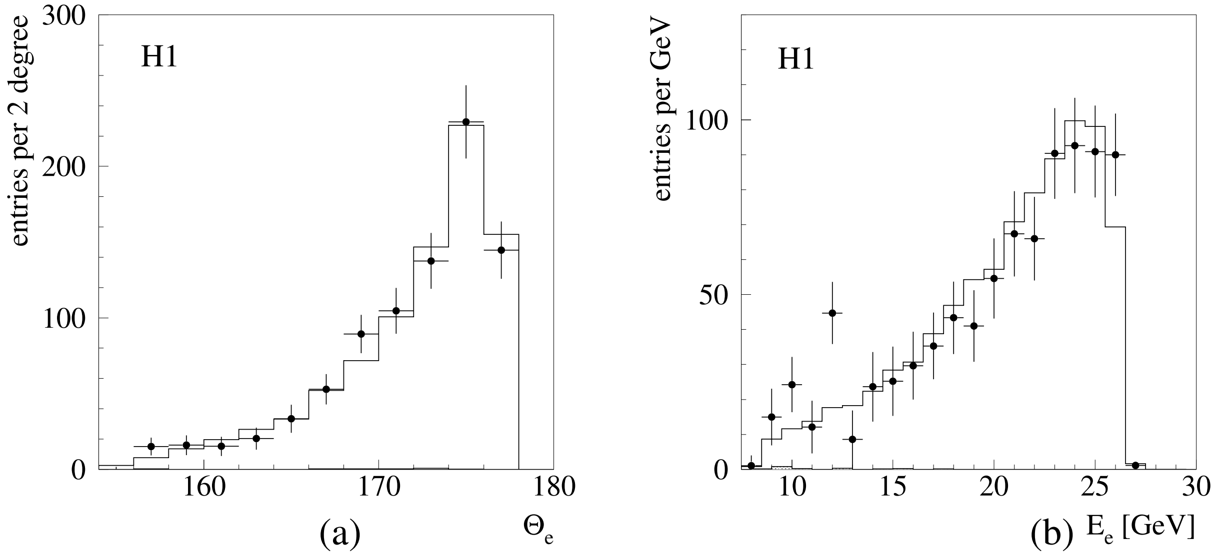

Figure 1: Distribution of (a) the polar angle and (b) the energy of the scattered positron for events with identified D^{*+} mesons. The data is compared with the absolute prediction of the AROMA Monte Carlo simulation (open histogram).

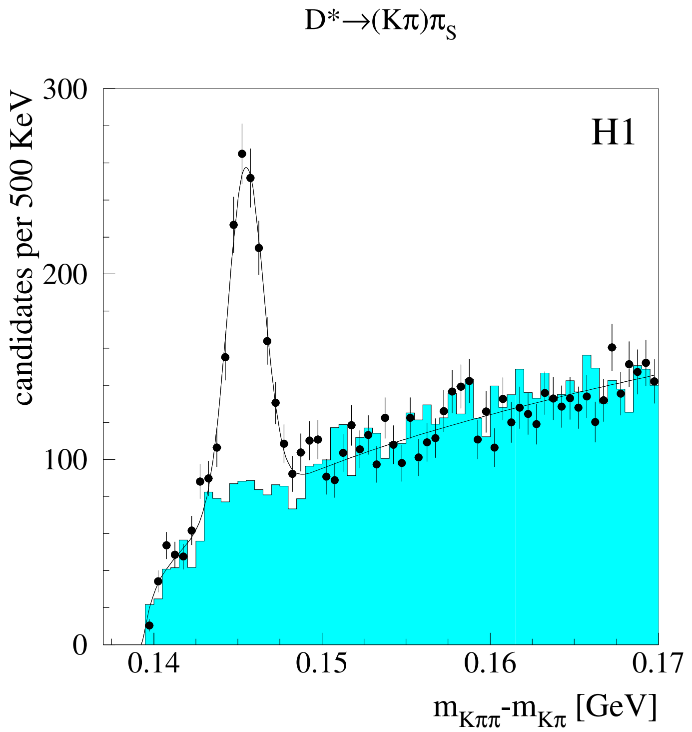

Figure 2: Distribution of the mass difference $\Delta m = m(K^-\pi^+\pi_s^+) - m(K^-\pi^+)$ for DIS events with D^* candidates. The data points are obtained from the $K^-\pi^+$ mass combinations fulfilling $|m(K^-\pi^+) - m_{D^0}| < 70$ MeV. The solid line represents the result of the fit described in the text. The shaded histogram shows the background expectation from the like sign $K\pi$ pairs.

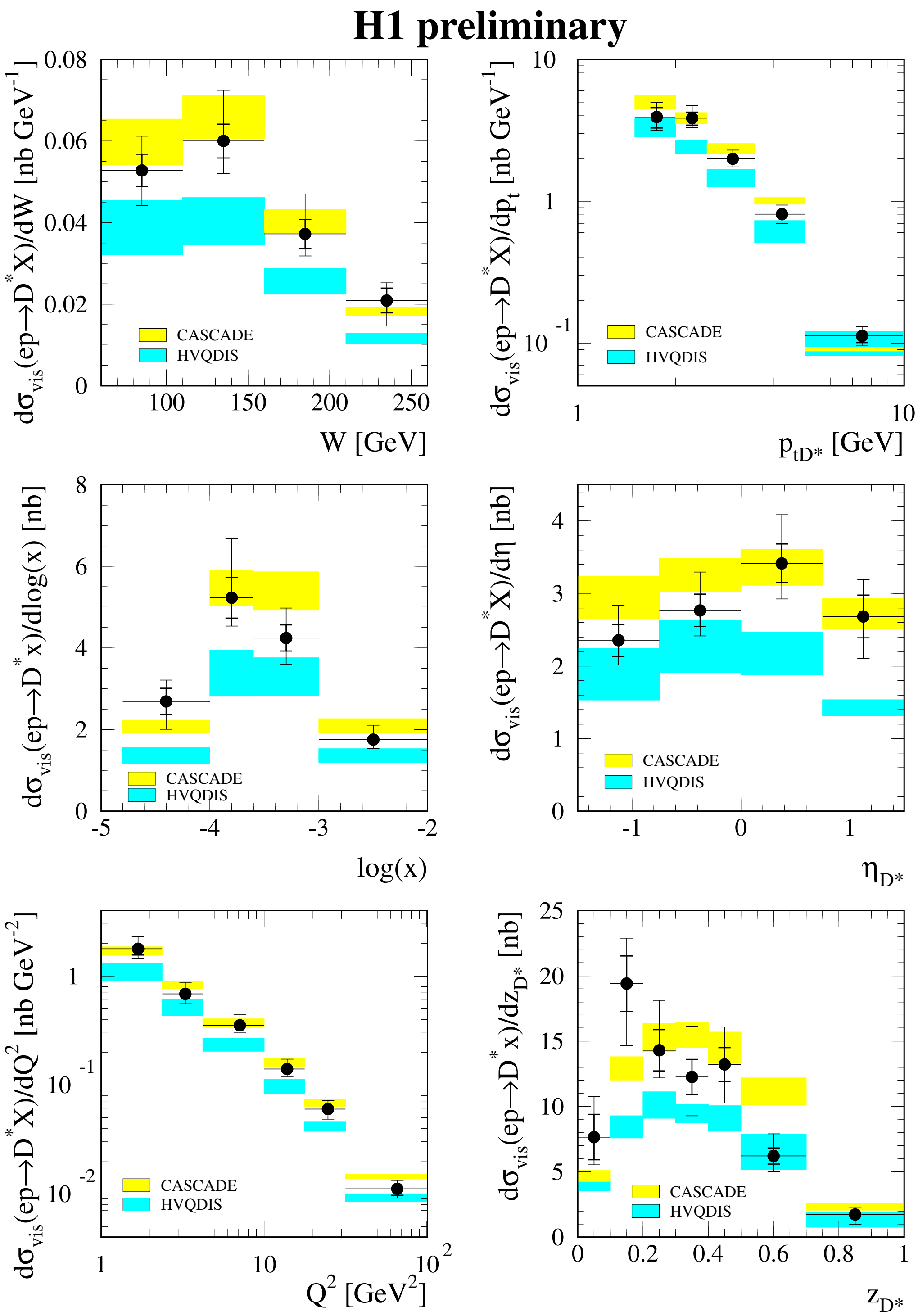

Figure 3: Single differential inclusive cross section $\sigma(ep \rightarrow eD^{*+}X)$ versus W, x_{Bj}, Q^2 and $p_{T\ D^*}$, η_{D^*}, z_{D^*}. The inner and outer error bars correspond to the statistical and the total errors. The expectation of the NLO DGLAP calculation using HVQDIS is indicated by the lower shaded band. The upper and lower bounds correspond to ($m_c = 1.3$ GeV, $\epsilon = 0.035$) and ($m_c = 1.5$ GeV, $\epsilon = 0.10$), respectively. The upper shaded band is the expectation of the CCFM calculations based on the CASCADE program. The upper and lower bounds correspond to $m_c = 1.3$ GeV and $m_c = 1.5$ GeV, respectively, with a fragmentation parameter of $\epsilon = 0.078$.

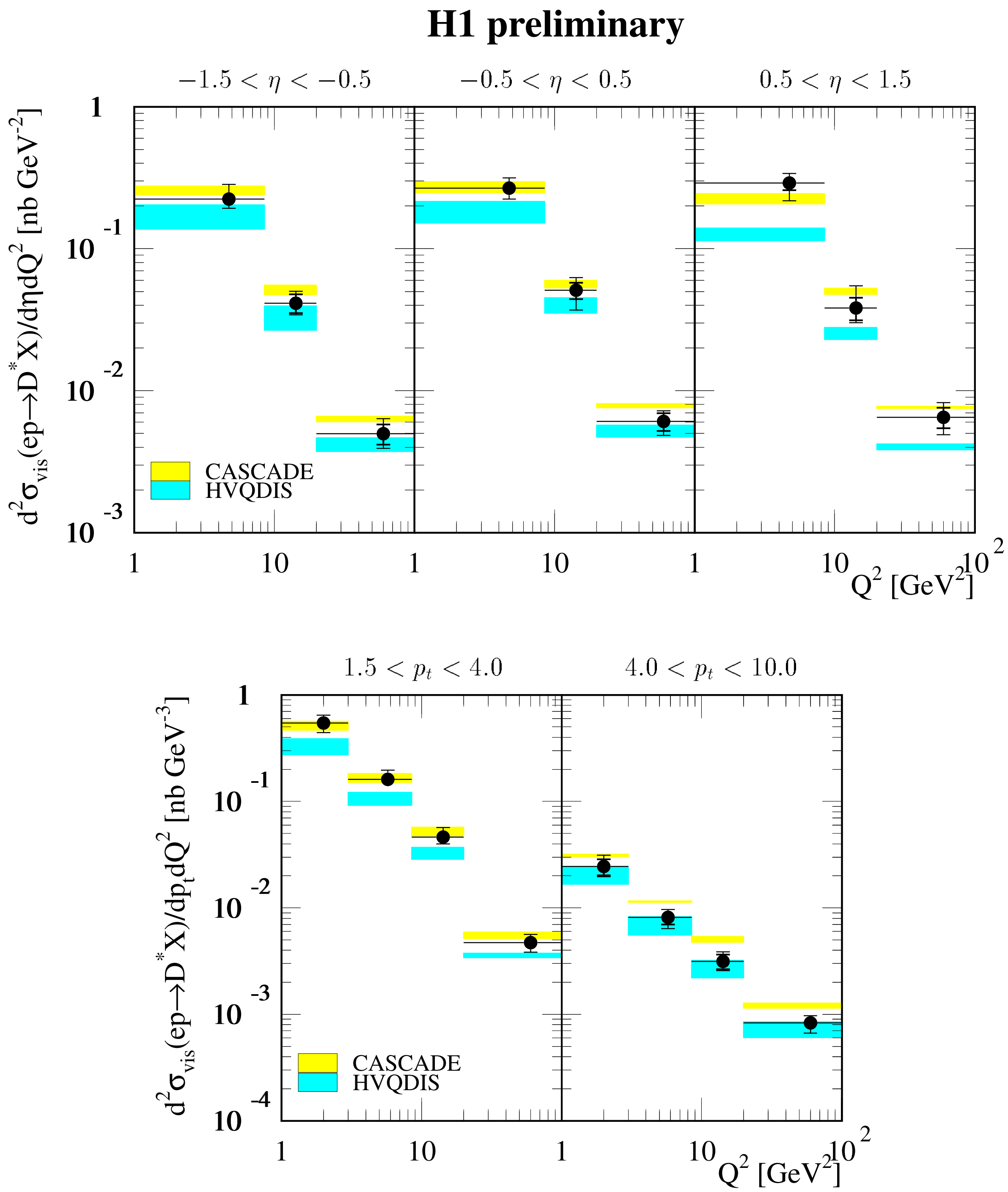

Figure 4: Double differential inclusive cross section $\mathrm{d}^2\sigma/\mathrm{d}\eta\mathrm{d}Q^2$ and $\mathrm{d}^2\sigma/\mathrm{d}p_t\mathrm{d}Q^2$ in bins of η and p_t. (See figure 3 for details)

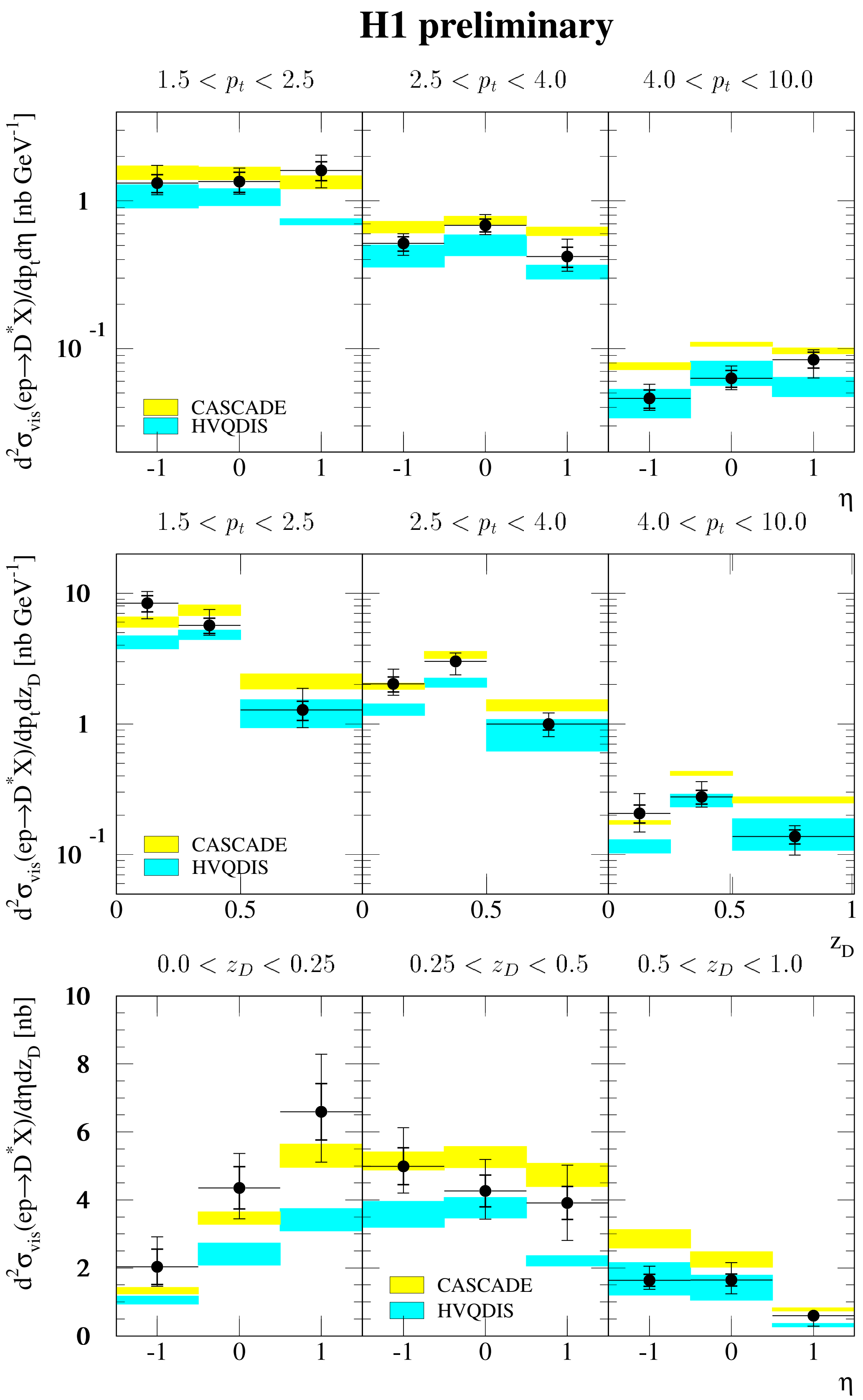

Figure 5: Double differential inclusive cross section $\mathrm{d}^2\sigma/\mathrm{d}p_t\mathrm{d}\eta$, $\mathrm{d}^2\sigma/\mathrm{d}p_t\mathrm{d}z_D$ in bins of p_t and $\mathrm{d}^2\sigma/\mathrm{d}\eta\mathrm{d}z_D$ in bins of η. (See figure 3 for details)

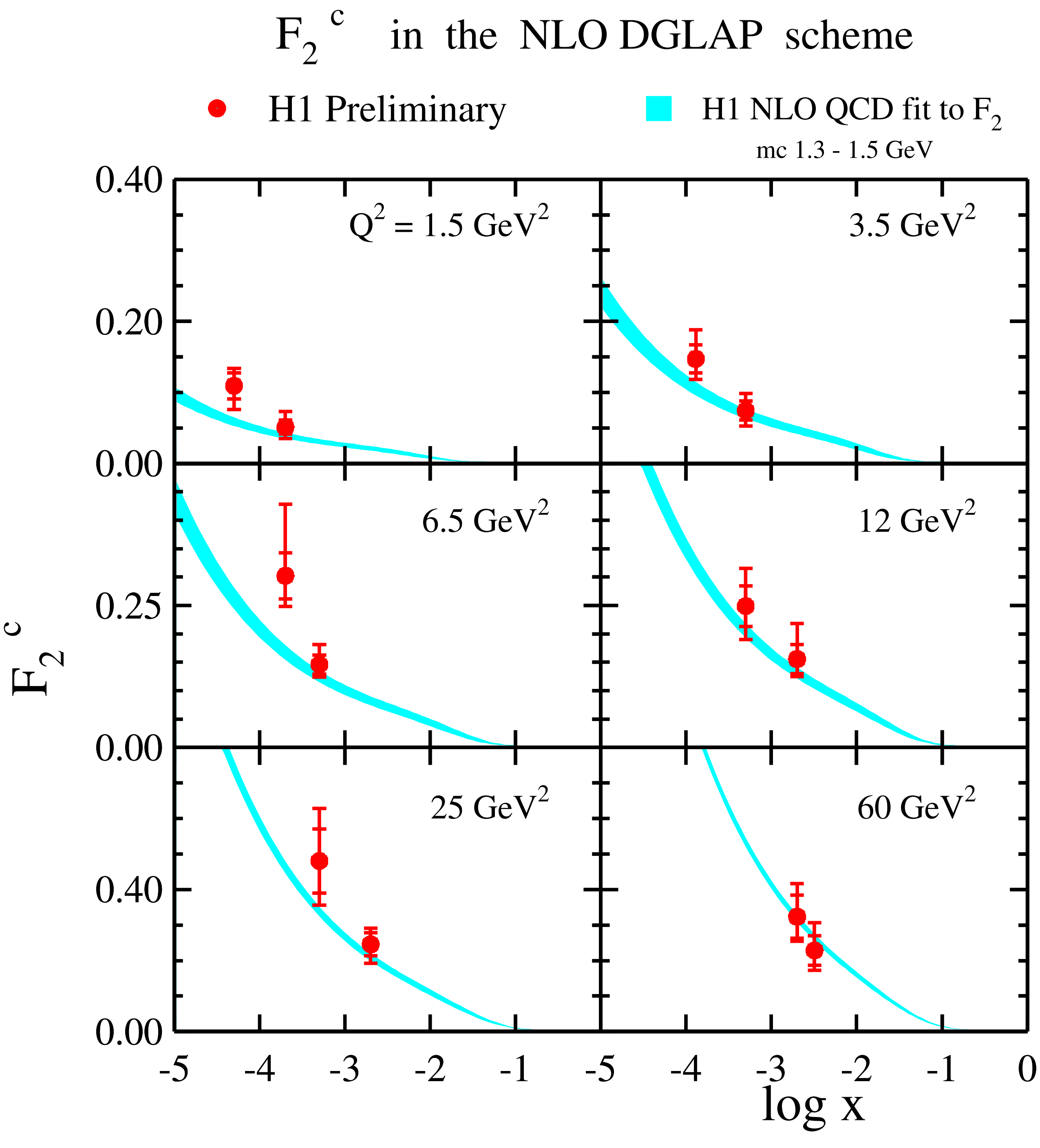

Figure 6: The charm contribution to the proton structure function F_2^c as derived from the inclusive D^{*+} meson analysis in the framework of DGLAP NLO for $m_c = 1.4$ GeV. The error bars refer to the statistical (inner) and the total error (outer), respectively. The shaded band represents the predictions of F_2^c from the H1 NLO DGLAP fit to the F_2 measurements ranging from $m_c = 1.3$ GeV to $m_c = 1.5$ GeV.

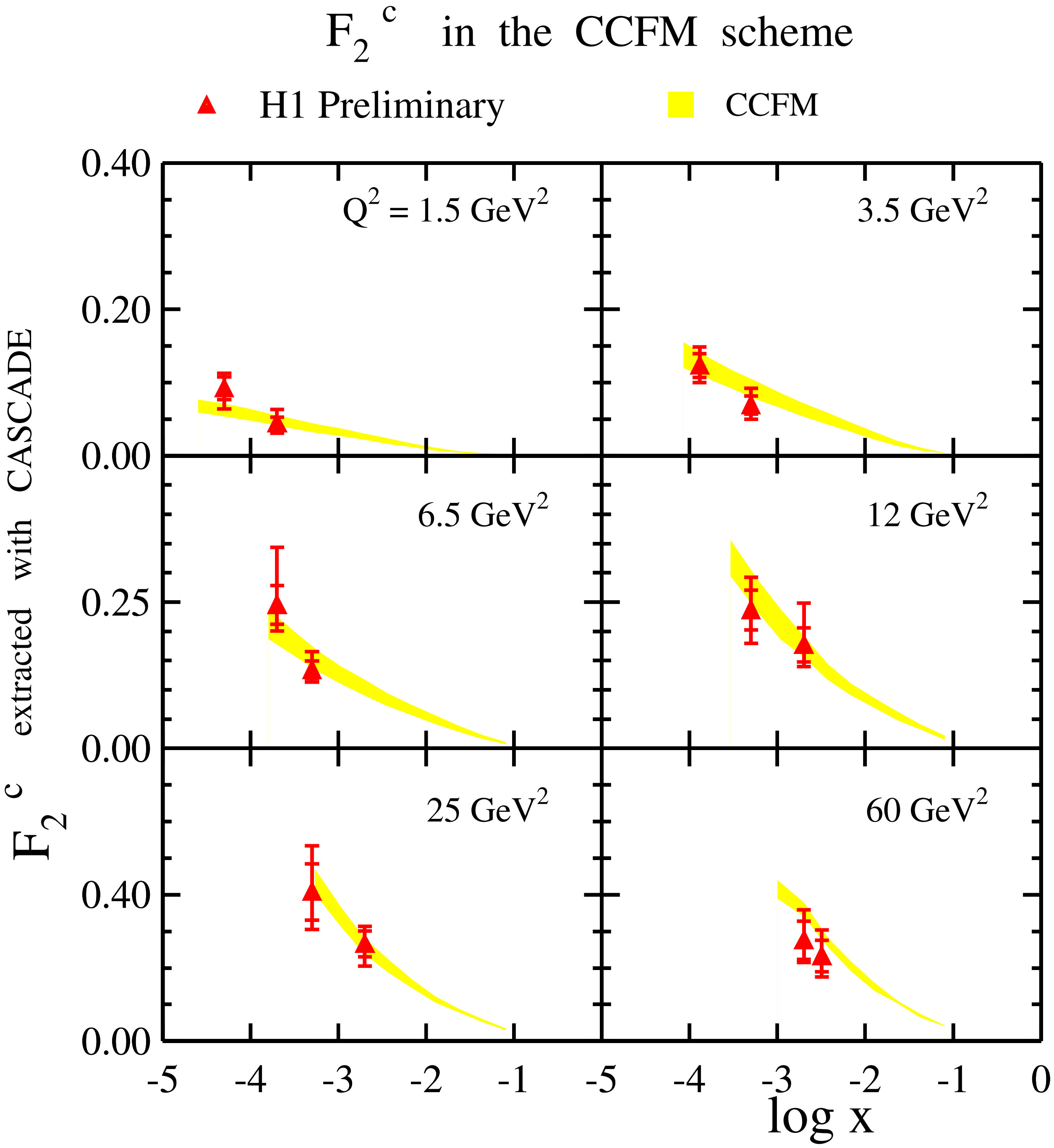

Figure 7: The charm contribution to the proton structure function F_2^c as derived from the inclusive D^{*+} meson in the framework of CCFM.The error bars refer to the statistical (inner) and the total error (outer), respectively. The shaded bands represent the CCFM predictions of F_2^c using a charm quark mass in the range from $m_c = 1.3$ GeV to $m_c = 1.5$ GeV.

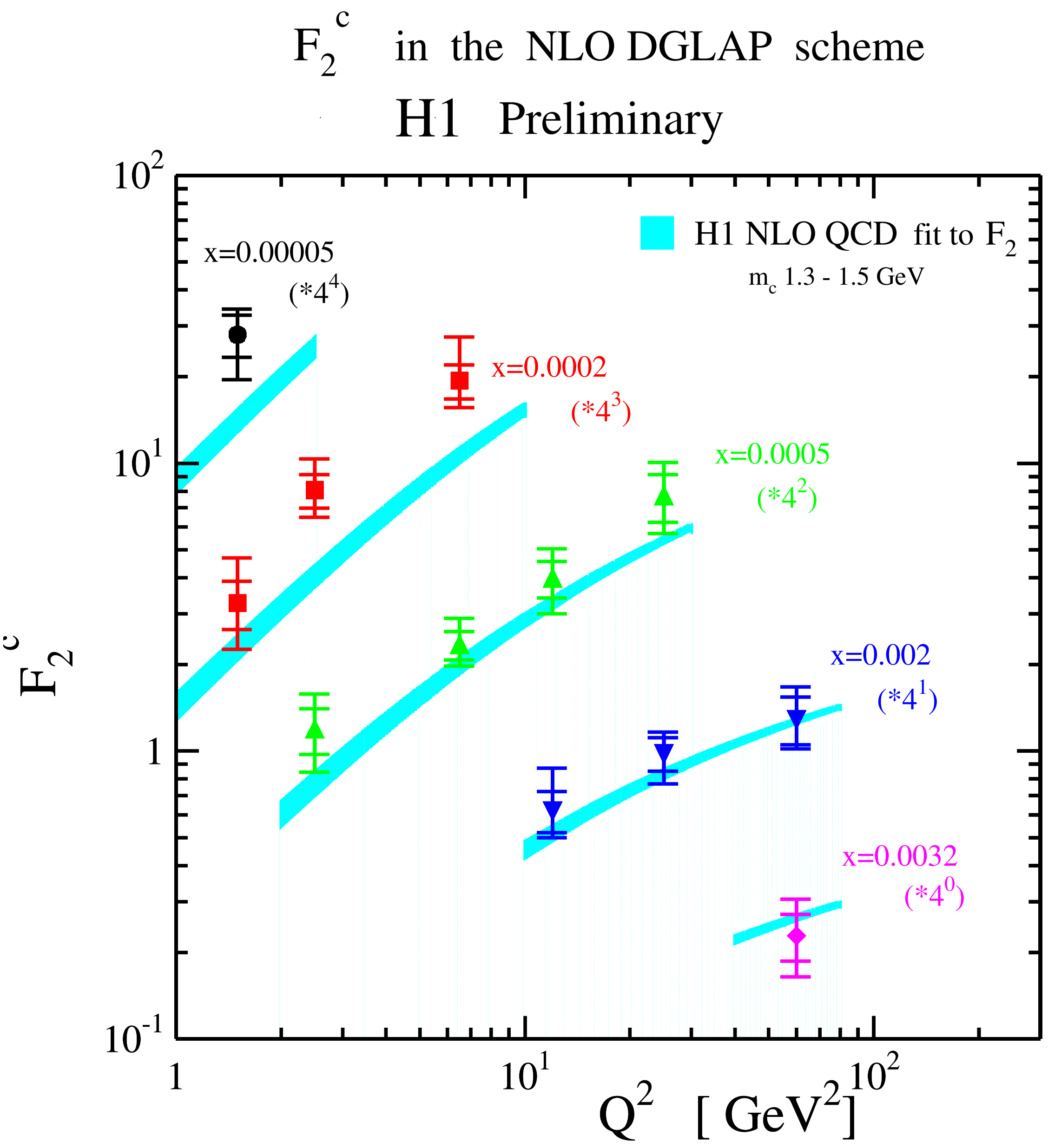

Figure 8: The charm contribution to the proton structure function F_2^c as derived from the inclusive D^{*+} meson as a function of Q^2 for different bins in x. The error bars refer to the statistical (inner) and the total error (outer), respectively. The shaded bands represent the predictions of the NLO DGLAP evolution based on the parton densities in the proton obtained by the NLO fit to the inclusive F_2.